CMTC-486215-MS

Stabilized CO_2 Foam for EOR Applications

Ahmed Farid Ibrahim, Arezoo Emrani, Hisham Nasraldin, Texas A&M University

This paper was prepared for presentation at the Carbon Management Technology Conference held in Houston, Texas, USA, 17-20 July 2017.

Abstract

The practice of injecting CO_2 for oil production was initiated in the 1950's. Today, CO_2 flooding is an established technique to enhance oil recovery (EOR), and CO_2 capture and storage in deep geologic formations is being studied for mitigating carbon emissions. CO_2-foam has been used to improve the sweep efficiency as a replacement for polymers to avoid formation damage. Although it is common to use surfactants to generate and stabilize foams, they tend to degrade at high temperatures (212°F), high-salinity environments, and in contact with crude oil. Adding nanoparticles is a new technique to stabilize CO_2 foams. The present work evaluates new foaming solutions that incorporate nanoparticles and viscosifiers to investigate the mobility-control performance when these foams are used as EOR fluids.

This study investigates the stability of alpha olefin sulfonate (AOS) foam and the corresponding mobility-reduction factor (MRF) for different foam solutions in the presence of nanoparticles and viscosifiers. To achieve this objective, foam stability was studied for various solutions to find the optimal solution at which higher foam stability in the CO_2 foam system can be reached. Coreflood tests were also conducted on different Buff Berea sandstone cores at 150˚F saturated initially with a dead crude oil. The CO_2 foam was injected with 80% quality as tertiary recovery mode. The oil recovery and the pressure drop across the core were then measured for different foam solutions.

Adding silica nanoparticles (0.1 wt%) and viscoelastic surfactant (VES) (0.4 wt%) to the AOS (0.5 wt%) solution improves both foam stability and MRF. In contact with crude oil, unstable oil-in-water emulsion formed inside the foam lamella that decreased the foam stability. A weak foam was formed for AOS solutions, but the foam stability increased by adding nanoparticles and VES. The oil recovery from the conventional water flooding (as a secondary recovery before foam injection) ranged from 40 to 48% of the original oil-in-place. AOS was not able to enhance the oil recovery with an apparent viscosity similar to that for the water/gas system (with no AOS in the solution), and no more oil was recovered by AOS foam. The addition of nanoparticles and VES to the solution improved the foam MRF and allowed extra oil production (8% in presence of nanoparticles, 15% by adding nanoparticles and VES).

Surfactants may not be able to stabilize foam at high temperatures and in contact with crude oil. Protecting surfactants from being degraded and improving the foam stability is of great importance and can be achieved by adding nanoparticles and viscosifiers to the solution. Adding nanoparticles is highly recommended for EOR applications, particularly at high temperatures.

Introduction

Carbon dioxide (CO_2) flooding has been used as an enhanced oil recovery (EOR) method. However, there are several challenges such as poor sweep efficiency and low oil recovery because of gravity segregation and viscous fingering. Moreover, the viscosity of CO_2-water/brine mixture without adding surfactant decreases as temperature increases (Chen et al. 2012). CO_2-foam has been investigated since 1960's to improve the sweep efficiency and oil recovery (Bian et al. 2012).

The first idea of using foam to displace oil was suggested and patented by Bond and Holbrook in 1958 (Wang and Li 2014). Fred (1961) conducted extensive laboratory experiments to further confirm that the foam can perform as a blocking agent to reduce the mobility of the displacing solvent (Wang and Li 2014). Based on Fred's work, the first idea to dissolve a surfactant into CO_2 during an EOR method for the purpose of mobility control foam was suggested by Bernard and Holm (1967) (Xing et al. 2012).

One of the interests of CO_2-EOR is to find surfactants soluble in CO_2 phase which can be injected with CO_2 to generate foam in reservoirs (Chen et al. 2012). The first surfactant families selected for EOR method was petroleum and synthetic aromatic sulfonates because of their availability and relatively low cost (Bavlere et al. 1988). For EOR process, the main requirement for using surfactants is to provide low interfacial tension (IFT) in multiphase systems formed in porous media.

CO_2-foam, consisting of low amounts of water and high amounts of compressed gas, minimize formation damage to unconventional reservoirs through fast cleanup and recovered permeability, as most of the gas flows back after depressurization (Xiao et al. 2016). However, CO_2-foams have some potential weaknesses. Foam stability improvement, especially in severe reservoir conditions, is a key factor to increase sweep efficiency. CO_2-foam can increase the viscosity of CO_2 relative to oil and water, which can cause improved sweep efficiency (Chen et al. 2012).

Foams are thermodynamically and kinetically unstable because the surface energy of gas/liquid interfaces tends to decrease as they degenerate into separate gas and liquid phases. At high-temperature reservoir conditions, surfactants generally tend to degrade. In addition, surfactant loss in a reservoir due to adsorption in the porous medium results in a large consumption of chemicals in CO_2-foam flooding. Thus, high reservoir temperature can be a major feature governing the economic viability of CO_2-foam flooding, and can also be another factor of foam instability (Chen et al. 2012).

The addition of thickeners such as polymers or VES for the CO_2-foam has been addressed to improve the foam stability (Zhao et al. 2015). Mixing surfactant and polymer may reduce fluid viscosity at high temperatures. However, adding nanoparticles to the mixture may enhance the liquid phase viscosity and stabilize CO_2-foam at high pressures and high temperatures (HP/HT). It is known that nanoparticles can adsorb at the gas/liquid interfaces to stabilize bubbles in foams by creating a rigid protective barrier around dispersed bubbles, which can reduce liquid film drainage.

Nanoparticles have been researched extensively as a means to stabilize foams used in oil production operations (Emrani and Nasr-El-Din 2017; Kalyanaraman et al. 2017; Singh et al. 2016; Mohd et al. 2014; and Mo et al. 2012). Nanoparticles are easily dispersed in water and able to flow through porous media (Mohd et al. 2014). Various other aspects of the nanoparticle-stabilized foams, such as the effect of salinity on the nanoparticle concentrations, have been established by Espinoza et al. (2010). They showed foam stability was improved as nanoparticle concentration increased under high salinity conditions. Although longer-lasting foams have been generated by various systems, the stability of these foams in the presence of crude oil and corefloods at high temperature has not been explored extensively. Yu et al. (2012) showed that the equilibrium adsorption of nanoparticles in different porous media is very low. Also, nanoparticles cannot change the core permeability based on their coreflood tests. They suggested that foam mobility increases with an increase of volumetric CO_2/nanoparticle dispersion phase ratio and injection flow rates. San et al. (2017) studied the effect of different ions on nanosilica-stabilized CO_2-foam generation. The results showed that stable CO_2-foam was generated as the synthetic produced water and nanosilica dispersion/CO_2 flowed through a porous medium (San et al. 2017).

Mixing surfactants can also improve the stability of foams especially in contact with crude oil (Andrianov et al. 2012). Mixing non-ionic surfactant to an anionic surfactant enhances the foam stability because of the formation of a viscous surface layer which raises the interfacial viscosity of the foam thereby reducing the rate of film thinning. Betaines are known for their foam enhancing properties generated a stronger and more stable foam in the presence of oil. Betaine increases the critical capillary pressure required for droplet entry which is related to the disjoining pressure, thus the foam stability increases (Basheva et al. 2000).

The capacity to reduce the gas-liquid mobility during the injection of foam into a porous media is known as foam blocking ability. The mobility reduction factor (MRF) is used as an index to indicate foam blocking ability and stability in this research. Therefore, large blocking ability represents a strong and stable foam (Wang et al. 2015).

The mobility reduction factor (MRF), defined as the ratio of total mobility of CO_2/brine to foam mobility, increases with the foam life. When foams become more stable, more resistance to flow results in a higher mobility reduction. Using CO_2-foam for mobility control was first proposed by Bond and Holbrook in 1958 (Yin et al. 2009). It has been proven that the addition of surfactants aid in the generation of foam wherever the CO_2 flows, especially if they are partially CO_2 soluble. The MRF can be calculated by comparing the pressure drop across the core during foam injection to the pressure drop measured at gas only (**Eq. 1**) (Bian et al. 2012):

$$\text{Mobility Reduction Factor} = \text{MRF} = \frac{\left[\frac{\text{k}\text{A}\Delta\text{p}}{\text{QL}}\right]_\text{f}}{\left[\frac{\text{k}\text{A}\Delta\text{p}}{\text{QL}}\right]_\text{g}} = \frac{\Delta\text{p}_\text{f}}{\Delta\text{p}_\text{g}}, \ldots\ldots\ldots\ldots\ldots\ldots\ldots\ldots\ldots\ldots\ldots\ldots\ldots\ldots\ldots\ldots.. \quad (1)$$

where Q is the flow rate, k is the absolute core permeability, A is the cross-section area of the core, L is the core length, μ is the viscosity, Δp is the pressure drop across the core. The subscripts “f” and “g” represent the experiment with and without foam, respectively.

The objective of this study is to investigate using nanoparticles and VES to improve foam properties and increase MRF in EOR applications. The experimental studies included: (1) foamability for different solutions combined with optical microscope analysis to examine the effect of the nanoparticles and VES on foam stability, and (2) coreflood tests to understand the effect of nanoparticles, VES in presence of oil on MRF.

Experimental Studies

Material. An anionic alpha-olefin sulfonate surfactant (AOS) was used to prepare the aqueous phase for a series of coreflood experiments. The general structure of this class of surfactants is $R\text{-}SO_3^-Na^+$, where (R) represents the hydrophobic group. The number of carbon atoms in the surfactant was 14-16 with an average molecular weight of 315 g/mol. The surfactant was obtained from a local chemical company as a solution containing 40 wt% active material. Foam solutions were prepared using brine containing 5 wt% NaCl in deionized water. CO_2 gas with a purity of 99.99 mol% was used to pressurize the system and form the foams under investigation. A chemical company supplied silica nanoparticles (SiO_2) of size 140 nm. Viscoelastic surfactant cocamidopropyl betaine (cocobetaine) (VES) was utilized to stabilize foam. The additives concentrations of the foam solutions were 0.5, 0.4, and 0.1 wt% for AOS, VES, and SiO_2, respectively. The solutions were mixed using a magnetic stirrer then homogenized with an ultrasonic homogenizer.

Berea sandstone cores were used with permeability ranging from 106 to 115 md. **Table 1** shows the mineralogy of the Berea sandstone cores. A dead crude oil was used in this study, and its properties are given in **Table 2.**

Mineral	Quartz	Kaolinite	Microline	Muscovite	Smectite
Concentration, wt%	91	3	4	1	1

Table 1 – Mineralogy of Berea sandstone cores.

Temperature, ℃	Viscosity, cp	Density, g/cm^3
25	3.03	0.82
30	2.44	0.81
40	2.04	0.81
50	1.71	0.80
60	1.88	0.79
70	1.61	0.78

Table 2 – The viscosity and density of dead crude oil.

Methods

Faomability Study. Foams are stabilized by surfactant-based solutions in the presence of a viscosifier or nanoparticles to prevent bubble coalescence. Foams are generally described in terms of their foamability, which is the ability of a foaming solution (surfactant only or surfactant with VES or nanoparticles) to form a foam. Foamability of the solutions was studied by performing a shake test.

Coreflood Study. The capacity to reduce the gas/liquid mobility during the injection of foam into a porous medium is known as foam blocking ability; hence the larger the blocking ability is, the more stable the foam would be. Mobility reduction factor (MRF) is used as an index to indicate foam blocking ability and stability in the present work.

Fig. 1 shows a schematic diagram of the coreflood setup used. Two stainless-steel piston accumulators with a capacity of two liters each were used to store the synthetic brine and the solutions (2). A one-liter accumulator was used to store the CO_2 (1) and was attached to a CO_2 cylinder (8). A syringe pump (7) was used to displace the solutions from the piston accumulators. Valves (v1, v3) were installed at the accumulator's outlet to control the fluids alternating during the injection. To monitor the pressure at the core inlet, a pressure gauge was installed at the coreholder inlet (G1). A hassler type core holder (3) was used to hold the core during the coreflood test. The coreholder was installed in an oven (11) that can be used to increase the system temperature. A backpressure regulator (10) was installed at the core outlet to maintain the outlet pressure. It was adjusted by a nitrogen cylinder (9). A hand pump (6) was used to apply overburden pressure around the core. A pressure transducer (4) was used to measure the pressure drop across the core and send the measurements to a data acquisition system (5) to a computer that records the data through a software.

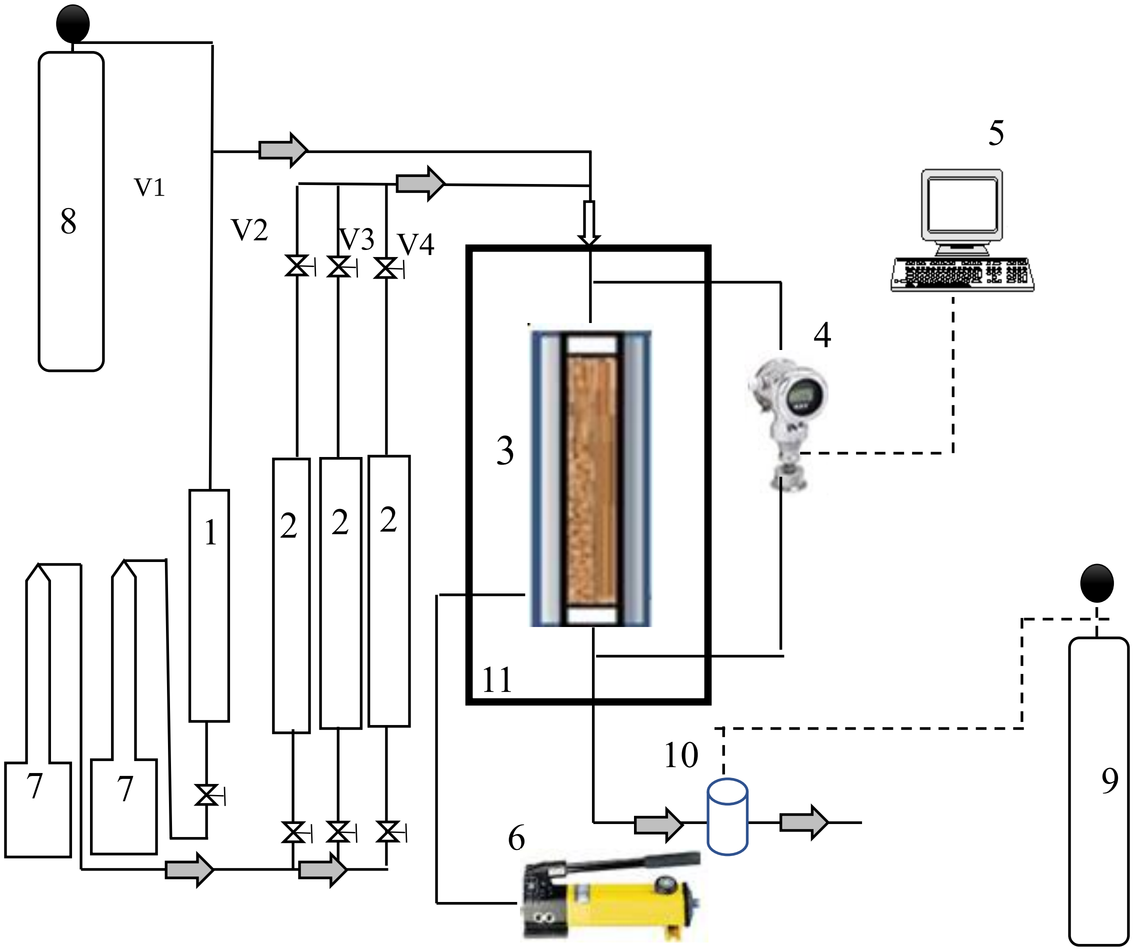

Fig. 1 – Schematic for coreflood setup, where 1 = CO_2 accumulator, 2 = brine and solution accumulators, 3 = core holder, 4 = pressure transducer, 5 = PC recorder, 6 = hand pump for overburden pressure, 7 = syringe pump, 8 = CO_2 cylinder, 9 = N_2 cylinder, and 10 = back pressure regulator, 11 = oven.

CT-Scan Analysis. X-ray computed tomography (CT) has emerged as a powerful tool for nondestructive imaging due to its simplicity and high-resolution images (Taud et al. 2005). When a CT scan is operated, the X-ray source rotates around the object and the transmitted X-ray intensity is recorded by a series of detectors. The recorded data is converted into numerical CT numbers. CT numbers are represented in Hounsfield units. A Hounsfield unit represents a relative change in the attenuation density. The scale is set so that air has a value of -1000, DI water is zero, and compacted bone is 1000.

Two different sample tubes were filled with the crude oil, and 5 wt% NaCl brine and scanned to obtain the CT number. CT for the NaCl brine and crude oil were estimated to be 66 and -170, respectively.

Core Preparation. Four cylindrical Buff Berea sandstone cores were used (6 in. length and 1.5 in. diameter). Each core was first dried in an oven at 150°F for 24 hrs. The weight of the dried core was measured (W_{dry}) and the core was scanned with computerized tomography (CT) scan (CT_{dry}). The core was then saturated with 5 wt% NaCl under vacuum for four hours. The core was then inserted on the coreholder and 5 wt% NaCl was injected at a constant flow rate at room temperature. Once the pressure drop across the core stabilized, the initial core permeability was measured. The weight of the saturated core was then measured ($W_{W\text{-}sat}$) and the core scanned again with CT scan ($CT_{W\text{-}sat}$). The core pore volume (PV) was calculated from the brine density (ρ_{brine} = 1.035 g/cm^3 at 70°F) and weight difference in both dry and saturated cases (**Eq. 2**). The cores were stored on the brine until it was time to run the experiment.

$$\mathrm{PV} = \frac{\mathrm{W_{W-sat}} - \mathrm{W_{dry}}}{\rho_{\mathrm{brine}}} \quad \text{……..…………………………………………………………………………} (2)$$

Where PV is the core pore volume, $\mathrm{W_{W-sat}}$ and W_{dry} are the core weight in brine saturated and dry cases, respectively. ρ_{brine} is the density of the brine, respectively.

Moreover, the porosity distribution along the core was estimated from the CT scan. The difference in the recorded CT number between the dry and saturated cases arises from the difference between both the brine and air density. This difference is proportional to the volume occupied by either fluid (pore volume), and estimation of the porosity can be calculated using **Eq. 3** (Akin and Kovscek 2003).

$$\emptyset = \frac{\mathrm{CT_{w-sat}} - \mathrm{CT_{dry}}}{\mathrm{CT_{brine}} - \mathrm{CT_{air}}} \quad \text{…………………………………………………………………………..} (3)$$

Where $\emptyset$ is the core porosity, $\mathrm{CT_{w-sat}}$ and $\mathrm{CT_{dry}}$ are the CT numbers of the core in brine saturated and dry cases, respectively. $\mathrm{CT_{brine}}$ and $\mathrm{CT_{air}}$ are the CT numbers of the brine and air, respectively.

Experiment procedures. **Fig. 2** shows schematic for the procedures of coreflood experiments. After pore volume and permeability measurements, the core saturated with the crude oil. The core inserted vertically on the core holder and the back pressure was set at 700 psi and the overburden pressure was set at 1500 psi. The oven temperature was set at 150°F. The crude oil was then injected at 0.2 $\mathrm{cm^3}$/min for 5 PV till no water is coming out then this step repeated at 0.5, 1 and 2 $\mathrm{cm^3}$/min for 2 PV to ensure reaching the maximum oil saturation. The initial oil inplace on the core is equal to the displaced water was collected. The weight of the oil-saturated core was measured ($\mathrm{W_{O\text{-}sat}}$) and the core was scanned with CT scan ($\mathrm{CT_{O\text{-}sat}}$). The initial oil inplace also confirmed from the weight difference between the water saturated and oil saturated cases (**Eq. 4**).

$$V_{oi} = \frac{\mathrm{W_{W-sat}} - \mathrm{W_{O-sat}}}{\rho_{\mathrm{brine}} - \rho_{\mathrm{oil}}} \quad \text{…………………………………………………………………………..} (4)$$

Where V_{oi} is the initial oil-in-place on the core, $\mathrm{W_{W-sat}}$ and $\mathrm{W_{O-sat}}$ are the core weight in brine saturated and oil saturated cases, respectively. ρ_{brine} and ρ_{oil} are the density of the brine and crude oil, respectively.

The initial oil saturation distribution along the core was estimated from the CT scan (**Eq. 5**).

$$S_{oi} = \left(\frac{\mathrm{CT_{w-sat}} - \mathrm{CT_{O-sat}}}{\mathrm{CT_{brine}} - \mathrm{CT}_{O}}\right) / \emptyset \quad \text{……………………………………………………………………….} (5)$$

Where S_{oi} and $\emptyset$ are the initial oil saturation and the core porosity, respectively. $\mathrm{CT_{w-sat}}$ and $\mathrm{CT_{O-sat}}$ are the CT numbers of the core in brine saturated and oil saturated cases, respectively. $\mathrm{CT_{brine}}$ and CT_{O} are the CT numbers of the brine and crude oil, respectively.

Water flooding stage was then followed as a secondary recovery mode. 5 wt% NaCl was injected at 0.5 $\mathrm{cm^3}$/min, and the produced oil collected with time for 5 PV until no oil observed on the production, then the flow rate increased to 1 and 2 $\mathrm{cm^3}$/min to ensure reaching the residual oil saturation. The weight of the water-flooded core was measured ($\mathrm{W_{W\text{-}flood}}$) and the core was scanned with CT scan ($\mathrm{CT_{w\text{-}flood}}$).

The total oil recovery from the water flooding was confirmed from the weight difference between the water flooded and oil saturated cases (**Eq. 6**).

$$V_{op-wf} = \frac{\mathrm{W_{W-flood}} - \mathrm{W_{O-sat}}}{\rho_{\mathrm{brine}} - \rho_{\mathrm{oil}}} \quad \text{……………………………………………………………………} (6)$$

Where V_{op-wf} is the total oil recovery from the water flooding, $W_{W-flood}$ and W_{O-sat} are the core weight in water flooded and oil saturated cases, respectively. ρ_{brine} and ρ_{oil} are the density of the brine and crude oil, respectively.

The residual oil saturation distribution along the core after water flooding was estimated from the CT scan (**Eq. 7**).

$$S_{or-wf} = \left(\frac{CT_{w-sat}-CT_{w-flood}}{CT_{brine}-CT_{O}}\right)/\emptyset \quad \ldots\ldots\ldots\ldots\ldots\ldots\ldots\ldots\ldots\ldots (7)$$

Where S_{or-wf} and $\emptyset$ are the residual oil saturation and the core porosity, respectively. CT_{w-sat} and $CT_{w-flood}$ are the CT numbers of the core in water-saturated and water-flooded cases, respectively. CT_{brine} and CT_{O} are the CT numbers of the brine and crude oil, respectively.

The last stage was the foam injection. On this stage, 5 wt% NaCl brine was injected first to pressurize the system and no more oil produced as it was a continuation of the water flooding stage. The foam solution was injected for two pore volumes to satisfy the adsorption requirements for the rock. CO_2 was then coinjected with the prepared foam solutions simultaneously to generate foam with 80% quality (gas volume / total volume = 80%). The foam was injected at 2 cm^3/min, and the produced oil collected with time for 5 PV where no more oil is producing. The weight of the foam-flooded core was measured ($W_{F\text{-}flood}$) and the core was scanned with CT scan ($CT_{F\text{-}flood}$).

Fig. 2 – Schematic for the procedures of coreflood experiments.

Table 3 shows the experimental design and physical properties of the cores that used on the core flood experiments.

Core #	Initial Core Permeability, md	PV, cm^3	Initial oil saturation vol%	Solution
1	113	32.4	57	5 wt% NaCl Brine
2	106	32.9	59.6	(0.5 wt%) AOS
3	110	33.3	57.6	(0.5 wt%) AOS + (0.1 wt%) SiO_2
4	115	33.4	61.8	(0.5 wt%) AOS + (0.4 wt%) VES+ (0.1 wt%) SiO_2

Table 3– Sandstone cores properties and the experimental conditions.

Results and Discussion

Shake test results. To generate foam, 5 cm^3 of the different foam solutions, (a) AOS solution, (b) a mixture of the AOS solution and SiO_2 nanoparticles, and (c) a mixture of the AOS solution, VES, and SiO_2 nanoparticles, were shaken at ambient conditions for one minute. **Fig. 3** shows the results of the foam shake test at 77°F and subsequent foam degradation over a time interval of 5 hours. In the absence of crude oil, a fine texture foam was generated, but the bubbles coalescence with time and the bubble size increased. The foam height remains unchanged with time for 5 hrs. on the three solutions. In presence of crude oil, the foam becomes unstable and decay very fast. AOS foam decayed in 30 min. The addition of nanoparticles to the AOS solution slightly increased the foam stability and the foam decayed completely in 1 hr. By adding VES to the foam solutions, the foam stability increased, where the foam remains for more than 5 hrs.

With Crude Oil				No Crude oil			
AOS + SiO_2 + VES	AOS + VES	AOS + SiO_2	AOS	AOS + SiO_2 + VES	AOS + SiO_2	AOS	Time
							0
							1 min
							5 min
							10 min
							30 min
							1 hr
							5 hrs

Fig. 3 – Foam shake test at 77°F for the different foam solutions in presence and absence of crude oil.

Two reasons for the deleterious effect of oil on the foam stability. First, the oil droplets tend to spread on the gas/liquid interface. As a result, the stable gas/liquid interface changes to unstable gas/oil interface, which accelerates the rupture of the foam lamella. Second, oil forms an emulsion on the foam lamella.

The oil droplets on the unstable emulsion agglomerate together and accelerate the drainage of the foam lamella, hence, the foam decays faster (Koczo et al. 1992).

Fig. 4 shows microscope picture for AOS foam in contact with crude oil. The crude oil forms layers on the interface between the gas and liquid phases. Moreover, an emulsion was formed inside the foam lamella. **Fig. 5** shows microscope pictures for the foam lamella in the case of AOS foam in the presence of oil. The oil droplets on the unstable emulsion agglomerate together and accelerate the drainage, where the lamella thickness decreases with time.

By adding nanoparticles and VES to the solution the foam becomes more stable. **Figs. 6** and **7** show the microscopic analysis for AOS, VES, and nanoparticles foam in contact with oil. The generated foam was stable, where the formed oil in water emulsion was very stable and remains dispersed. As a result, the foam lamella thickness didn't change with time and the foam lasts for a longer time as appears on the shaking tests.

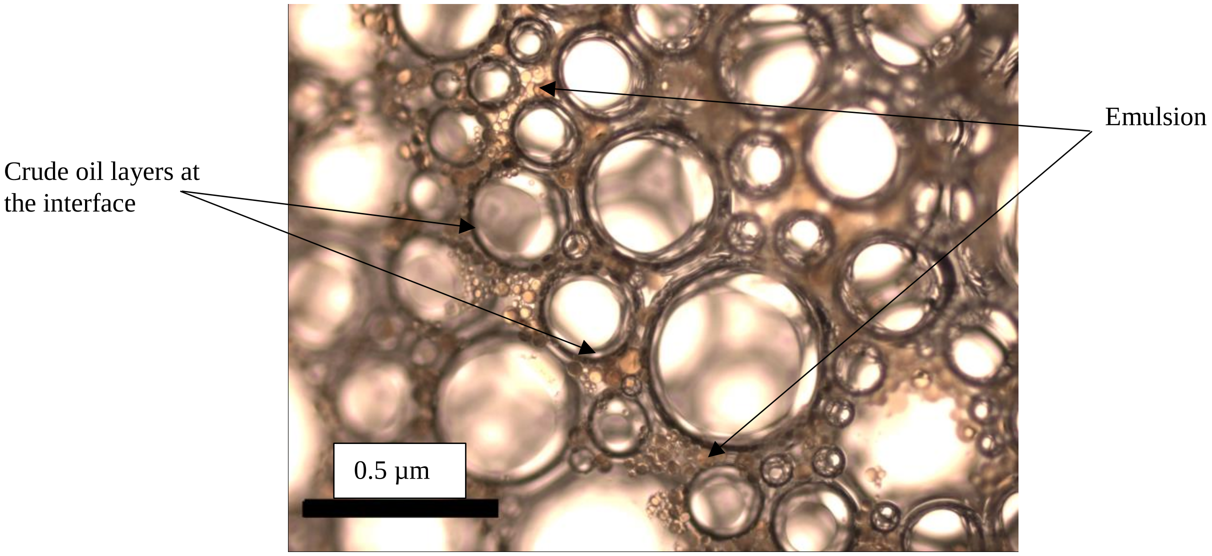

Fig. 4 – Microscope analysis for AOS foam in contact with oil (5x).

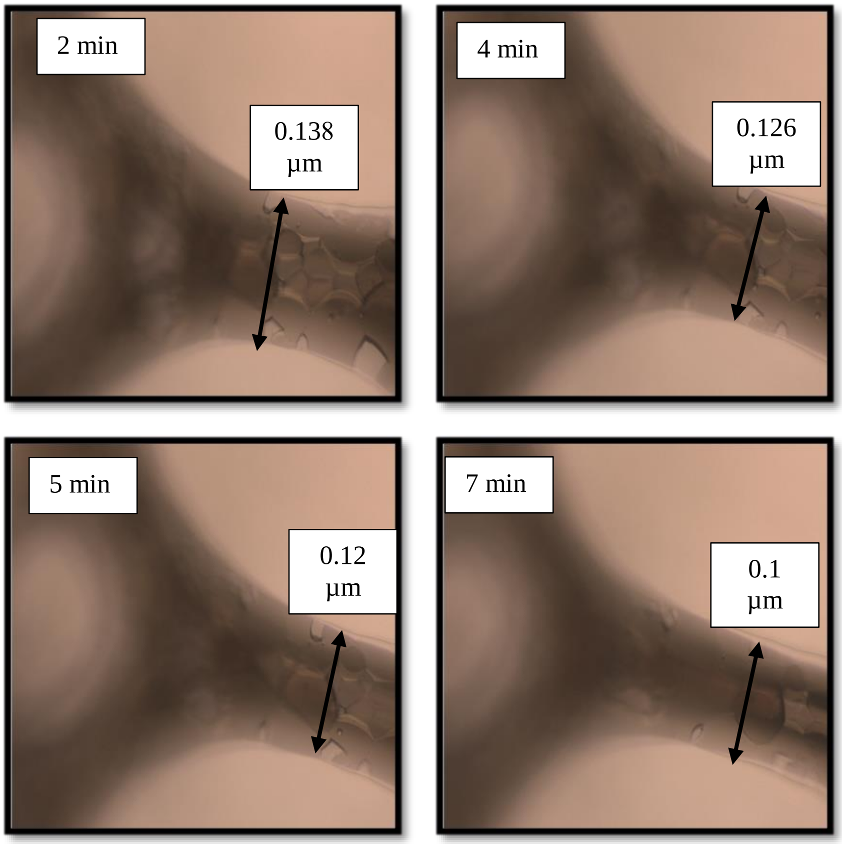

Fig. 5 – Microscope analysis for AOS foam to track the unstable emulsion and draining of the foam lamella with time in contact with oil (20x).

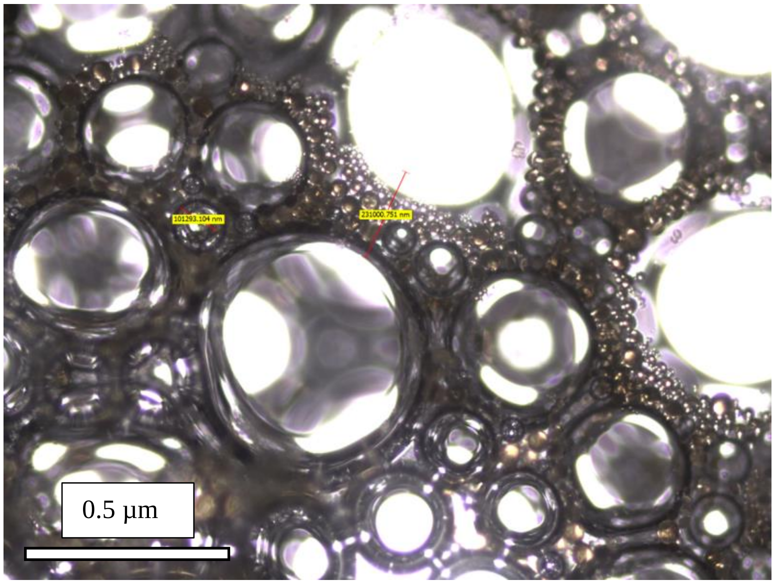

Fig. 6 – Microscope analysis for AOS, VES, and nanoparticles foam in contact with oil (5x).

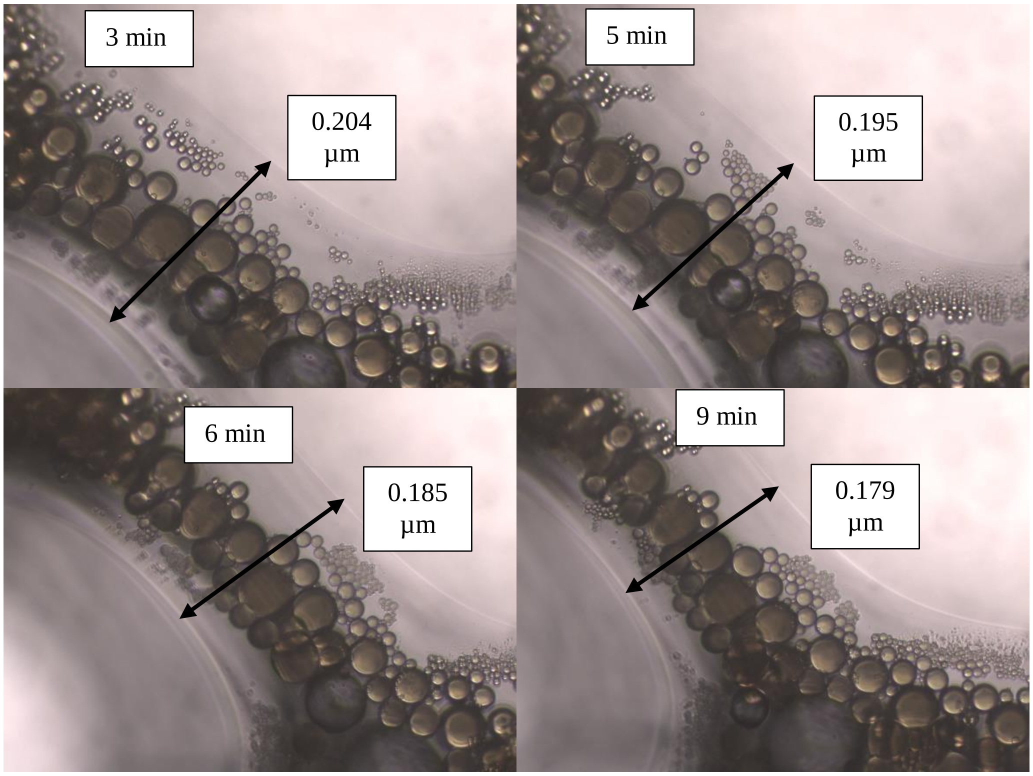

Fig. 7 – Microscope analysis for AOS, VES, and nanoparticles foam to track the emulsion and draining of the foam lamella with time in contact with oil (20x).

Coreflood results. Four coreflood experiments were conducted to emphasize the effect of adding nanoparticles and VES on the foam stability and the EOR performance. The initial oil saturation in the four cores varied between 57 to 61.8 vol% with initial oil-in-place between 18.5 to 20.6 cm^3. The oil recovery from the water recovery as a secondary mode was between 40 to 48 % of the initial oil-in-place and residual oil saturation 30 to 35 vol%. **Fig. 8** shows the CT scan along core #3 for different cases including dry, water-saturated, oil-saturated, and water-flooded cases. The CT number values increase the density of the fluids on the pores increases. Lowest values appeared on the dry case where the pores filled with air, and highest values in the case of the water-saturated core where the pores filled with brine. As the water replaced with oil in oil-saturated case, the CT number values decreased due to low oil density (0.82 g/cm^3) comparing to brine density (1.035 g/cm^3). Finally, by water flooding and displacing the oil from the pores, the CT number values increased but did not reach the water-saturated case due to the presence or residual oil in the pores. Eqs. 3, 5, and 7 was used to calculate the porosity, initial, residual oil saturations along the core. **Fig. 9** shows the porosity, initial, and residual oil saturations distribution along the core. The average core porosity was 18.9 vol%. For the oil saturation stage (primary drainage), the crude oil was injected at different flow rates until no water was observed on the outlet flow to ensure reaching the residual water saturation. The oil saturation trend shows higher oil saturation at the inlet than that at the outlet due to viscous fingering. The same behavior was found in the case of the residual oil saturation after water flooding. **Fig. 10** shows the pressure drop across the core at different injection rates (0.5 to 2 cm^3/min) and the corresponding recovery factor during the water flooding stage. At 0.5 cm3/min, most of the oil was produced (recovery factor = 49%) and then the recovery factor slightly increased (50%) after the flow rate increased to 1 cm3/min.

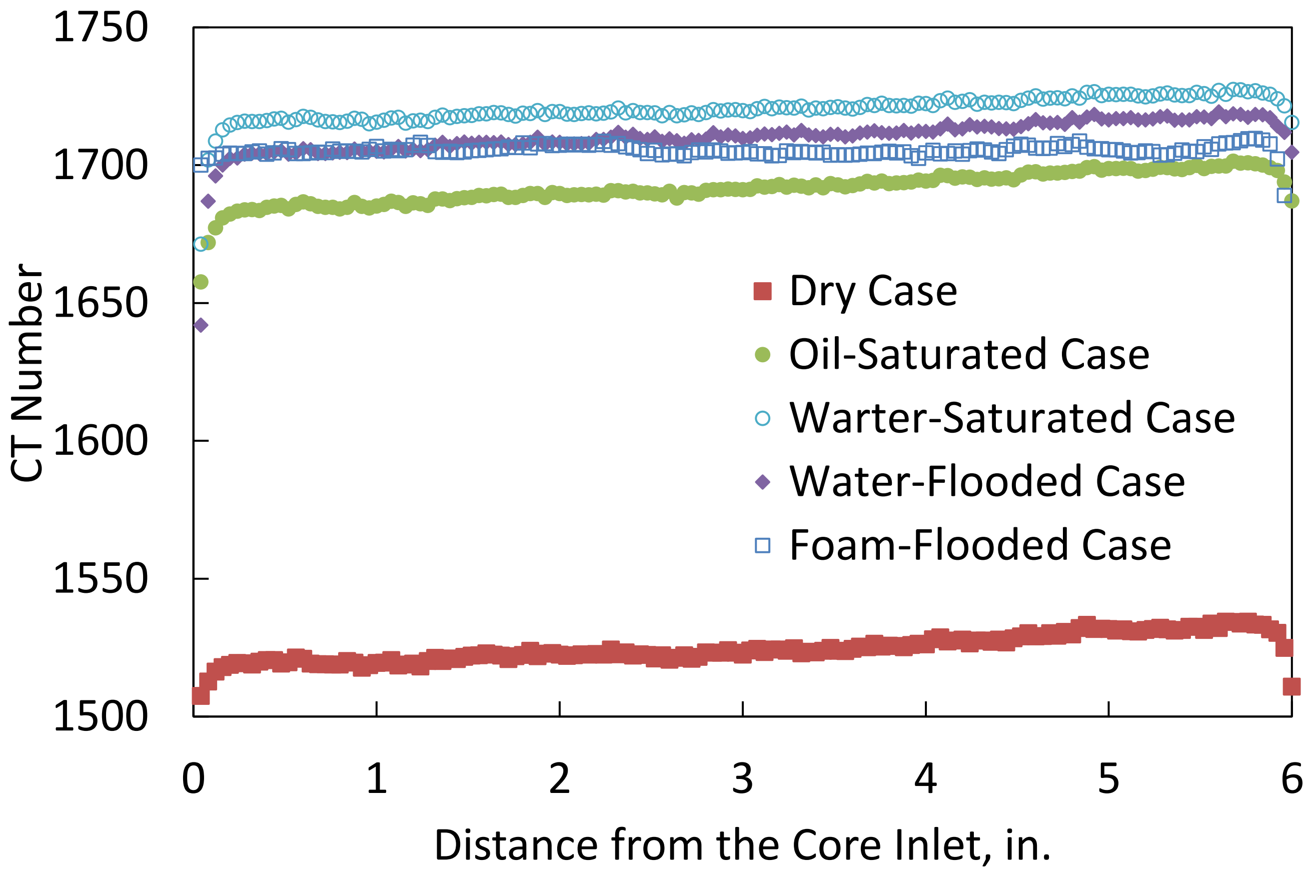

Fig. 8 - CT scan trend along core #3 for different cases.

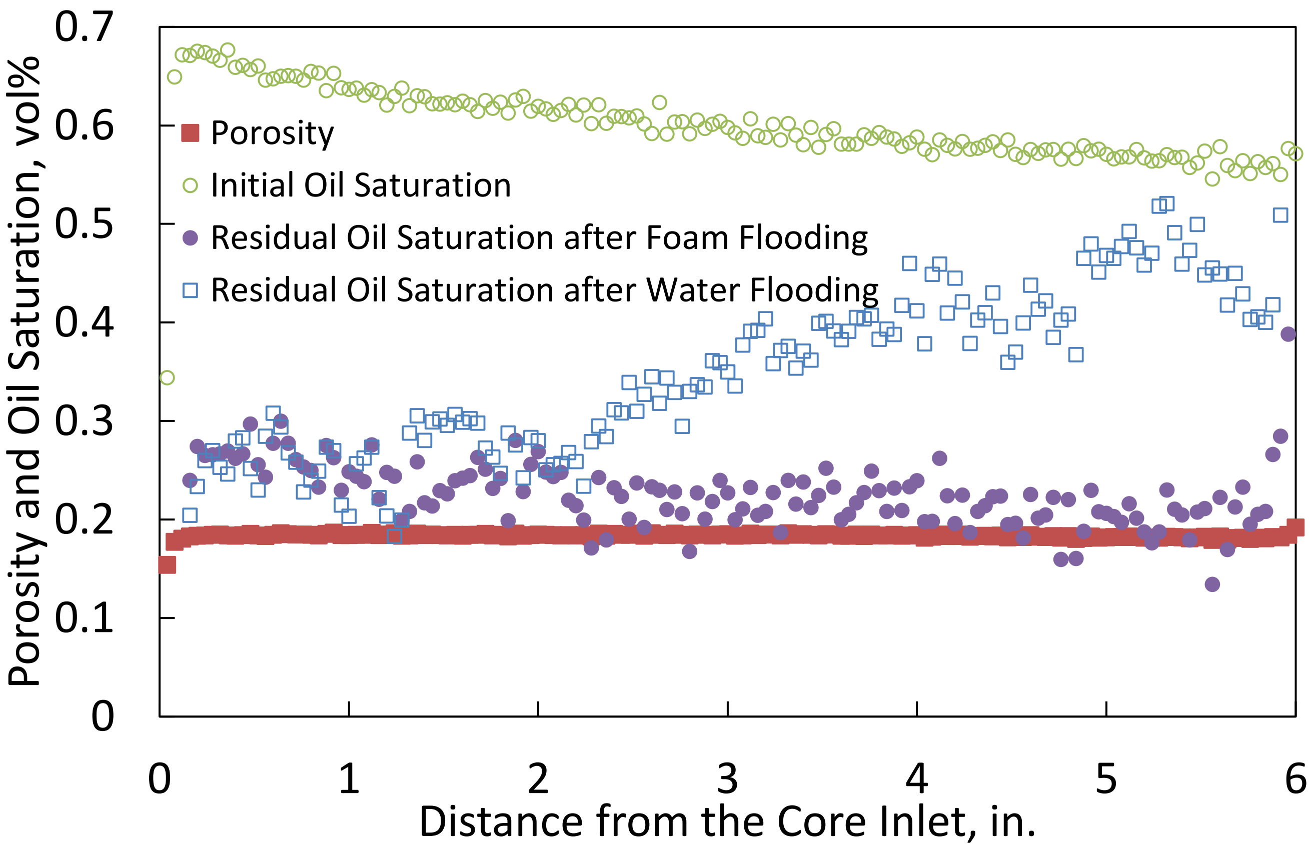

Fig. 9 – Porosity, initial, and residual oil saturations distribution along the core.

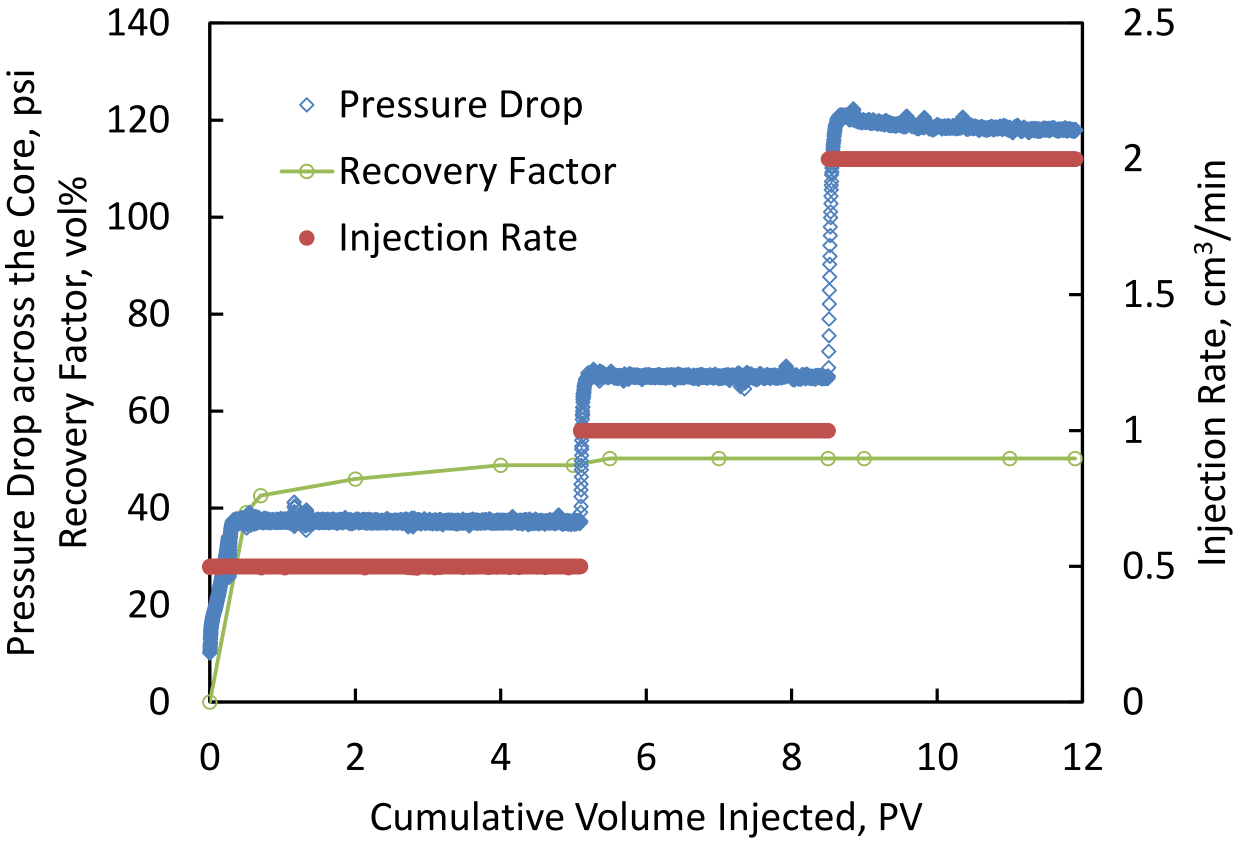

Fig. 10 – Pressure drop across the core at different injection rates and the corresponding recovery factor during the water flooding stage.

Fig. 11 shows the pressure drop across the core for the coreflood experiments during the tertiary recovery mode. **Fig. 12** shows the recovery factor from the tertiary mode (oil recovery/oil-in-place before foam injection). The pressure drop is an indication for the mobility control factor as defined by Eq. 1. Lower pressure drop was observed on the first core, where CO_2 was coinjected with NaCl brine with no foam generation and only 29.6% of the residual oil after water flooding was produced. The reason for that is the viscosity fingering and lower displacement efficiency. With adding 0.5 wt% AOS, a weak foam was generated and the pressure drop slightly increased. Hence, the AOS did not control the gas mobility. As a result, AOS was not able to enhance the oil recovery with an apparent viscosity similar to that for the water-alternative-gas system (with no AOS in the solution). Oil recovery from the AOS foam increased by 2% compared to the water/gas system.

The pressure drop across the core increased in the presence of nanoparticles in the solution, which indicates increasing the mobility control factor. Emrani et al. (2017) explained that the nanoparticles adsorb to the interface between the liquid/gas phases and minimizes the contact area between them; as a consequence, it can build a strict barrier that prevents droplets coalescence and improves the foam stability. Increasing the mobility reduction factor reflects improving the displacement efficiency. As a result, the oil recovery increased (38% of the residual oil after water flooding).

Adding VES to the system stabilizes the emulsion and delay the foam decay that improves the foam stability as shown from the foamability tests. Therefore, mobility reduction factor improved and the oil recovery increased to 45.7% as well. Moreover, adding VES to the foam solutions increases the liquid viscosity, and the viscosity slows down the drainage of liquid initially. This keeps the liquid film thicker and causes the foam to stay in a stable state for a longer time.

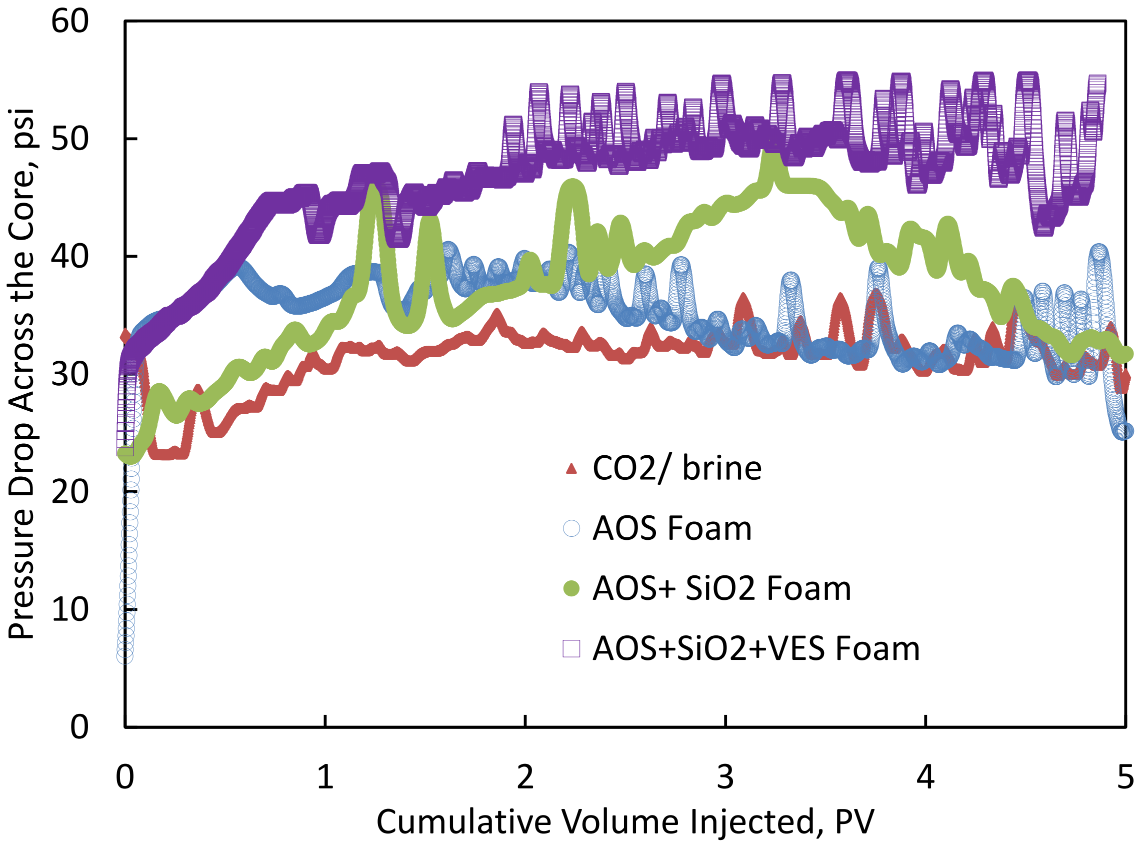

Fig. 11 – Pressure drop across the core during the tertiary recovery mode.

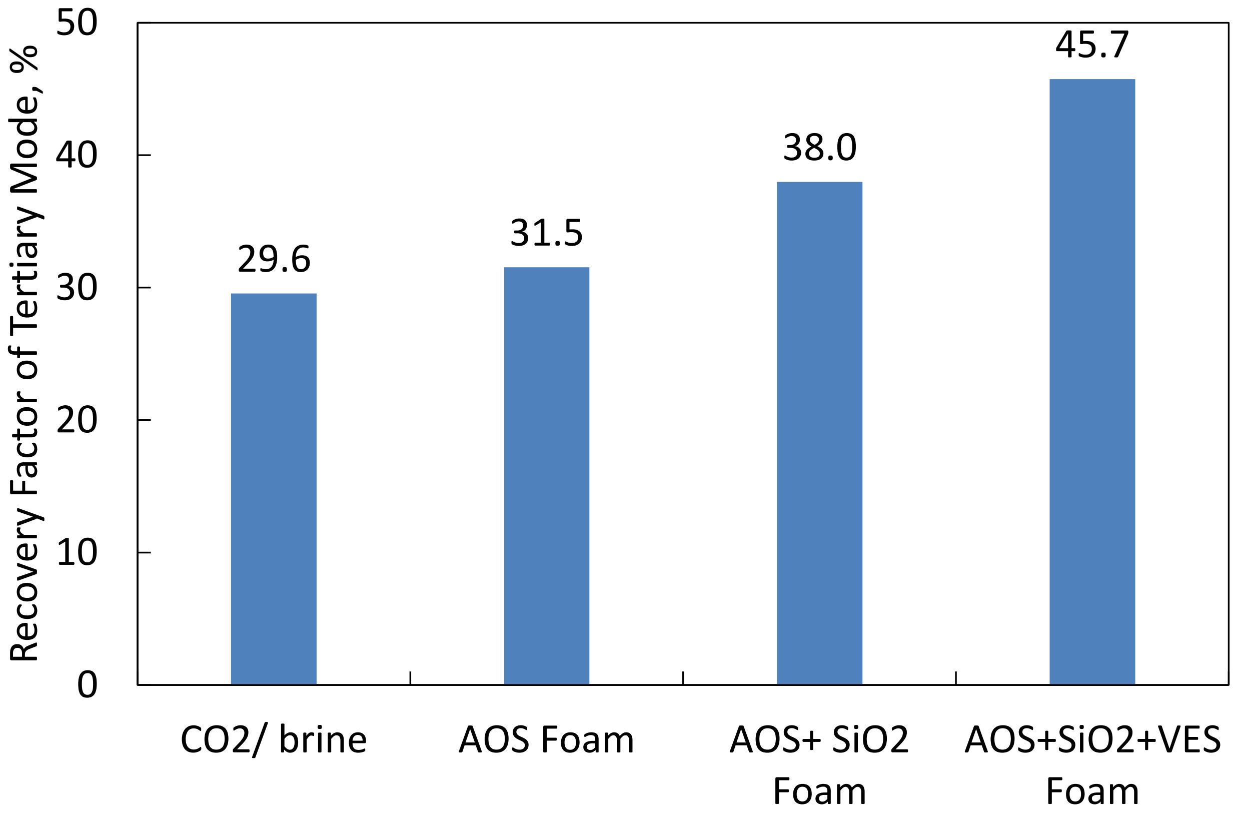

Fig. 12 – Recovery factor from the tertiary recovery mode for the different foam solutions.

Fig. 13 summarizes the CT scan results for the four cores on the different injection stages. CT number values varies from 1400 to 1950. The lower CT values indicated by blue color and as the CT number increase, it changes to red then white. In the dry case, the cores had the lowest CT number where the pores were filled with air with CT number of (-1000). However, the water saturated cores had the highest CT number, where the pores were filled with brine with CT number of (66). The other three cases (oil-saturated, water-flooded, and foam flooded cases) the pores were filled with oil and brine, as a result, the CT number will be between water-saturated and dried cases (oil CT number is -170). As the oil saturation increases, the core CT number decreases and the color will tend to blue. CT scan images in the case of core 1 and 2 after foam flooding indicate lower displacement efficiency and more crude oil left behind. As the foam quality increases in the case of nanoparticles and VES, the displacement efficiency increases and the residual oil decreases.

	Dried case	Water Saturated case	Oil Saturated case	Water Flooded case	Foam Flooded case
Core 1 (CO_2/Brine)	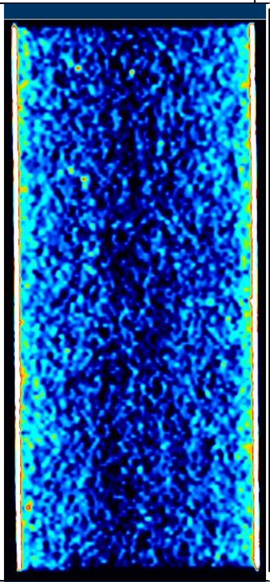	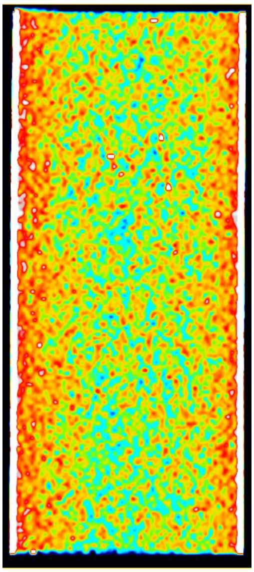	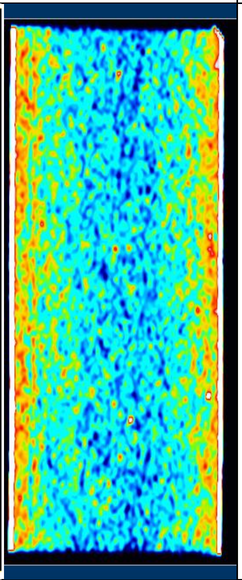	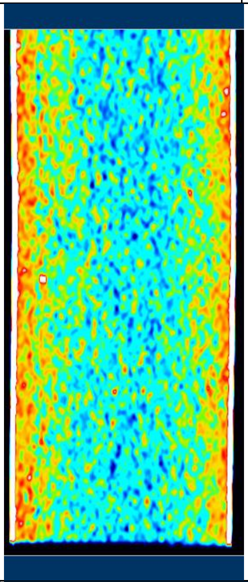	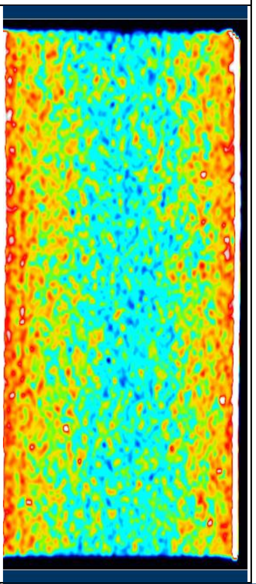
Core 2(CO_2/AOS Solution)	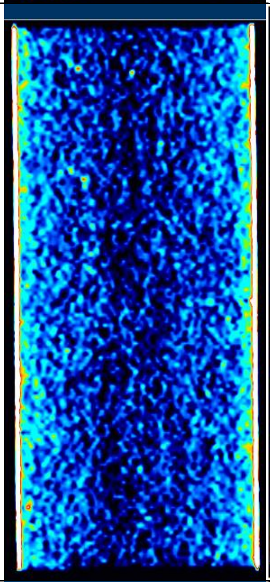	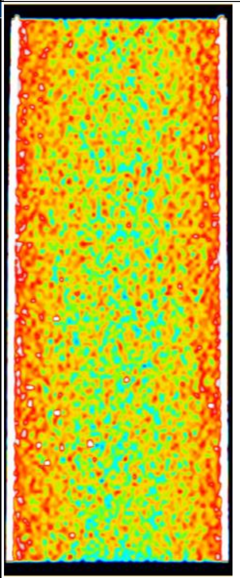	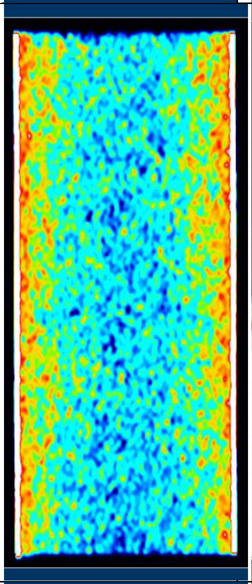	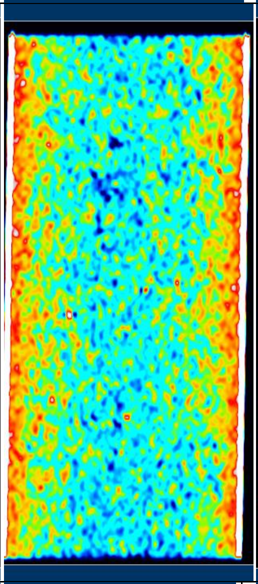	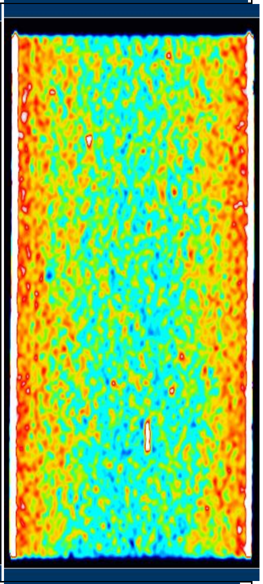
Core 3 (CO_2/AOS+SiO_2 Solution)	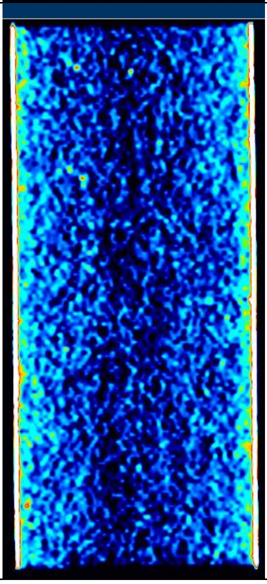	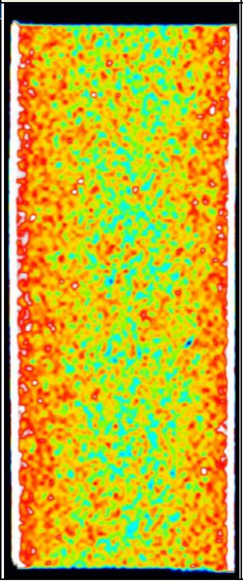	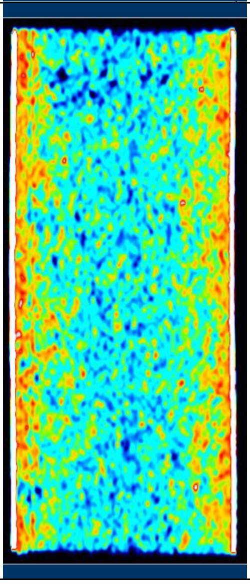	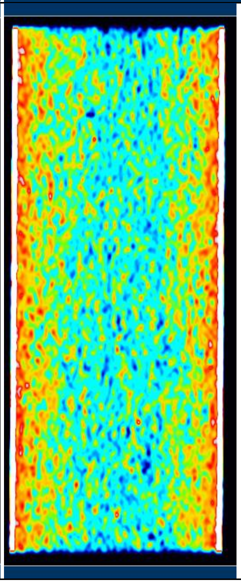	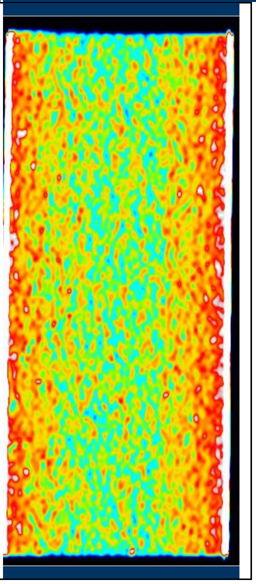

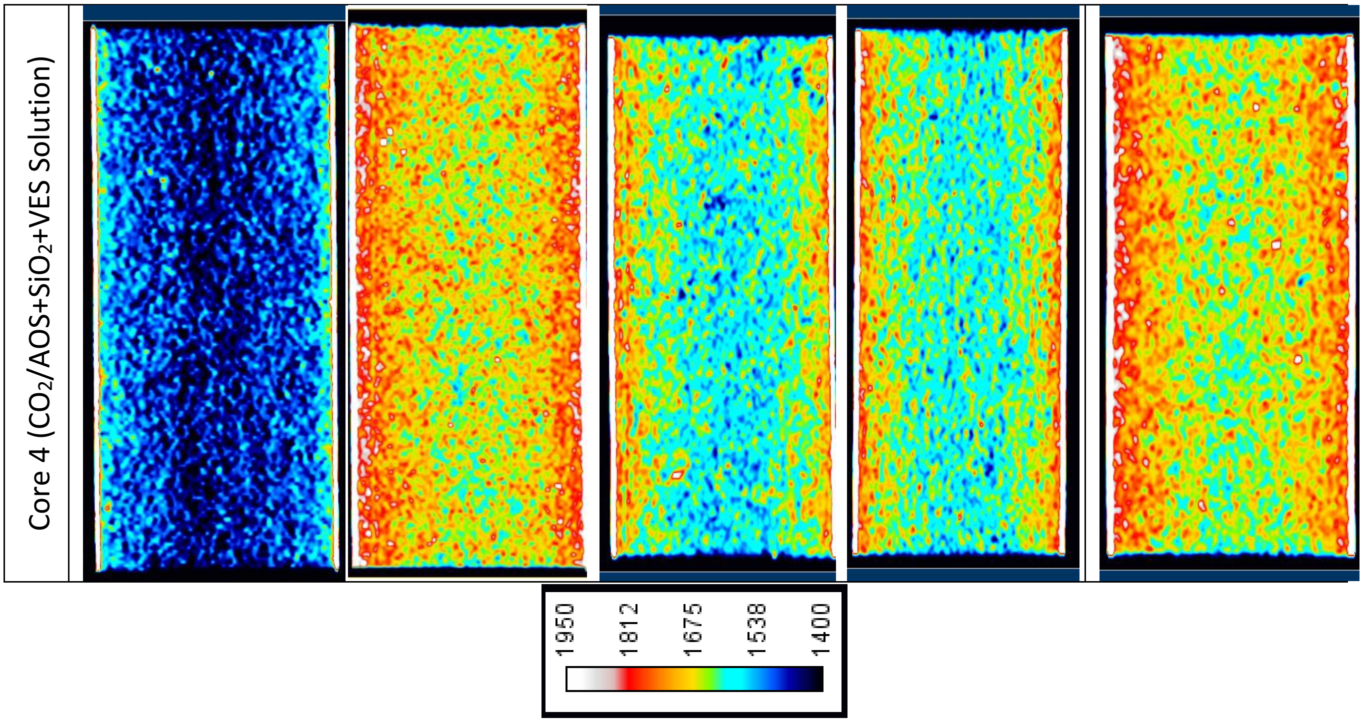

Fig. 13 – CT scan analysis for the different foam solutions after the different injection stages.

Conclusions

This study investigates the effect of VES and silica nanoparticles on foam stability and MRF in porous media. The main conclusions are summarized as follows:

1. Adding silica nanoparticles and viscoelastic surfactant to the AOS solution improves both foam stability and MRF.
2. In contact with crude oil, unstable oil-in-water emulsion formed inside the foam lamella and oil layer formed on the gas/liquid interface that decreased the foam stability and accelerates the lamella drainage.
3. A weak foam was formed for AOS solutions, but the foam stability increased by adding nanoparticles and VES.
4. AOS was not able to enhance oil recovery with an apparent viscosity similar to that for the water-alternative-gas system (with no AOS in the solution), and almost no more oil was recovered by AOS foam.
5. The addition of nanoparticles and VES to the solution improved the foam MRF and allowed extra oil production (8% in the presence of nanoparticles, 15% by adding nanoparticles and VES).

Acknowledgements

The authors thank the Crisman Institute and Texas A&M University for its support to conduct this work.

Abbreviations

AOS	alpha olefin sulfonate
EOR	enhanced oil recovery
HT	high temperature
HP	high pressure
MRF	mobility reduction factor
VES	viscoelastic surfactant

CT	computed tomography
PV	core pore volume

Nomenclature

A	cross-section area of the core, cm^2
K	absolute core permeability, md
L	core length, in.
Q	total flow rate, cm^3/min
S	fluid saturation, volume fraction
V	oil volume, cm^3
W	core weight, gm
ρ_{brine}	brine density, g/cm^3
$\emptyset$	core porosity, volume fraction
Δp	pressure drop across the core, psi
μ	fluid viscosity, cp

Subscripts

w	water
o	oil
w-_{flood}	water flooding
r	residual

References

Akin, S., and Kovscek, A. R. 2003. Computed tomography in petroleum engineering research. Geological Society, London, Special Publications. 215 (01): 23-38. https://doi.org/10.1144/GSL.SP.2003.215.01.03.

Andrianov, A., Farajzadeh, R., Mahmoodi Nick, M. et al. 2012. Immiscible Foam for Enhancing Oil Recovery: Bulk and Porous Media Experiments. *Industrial & Engineering Chemistry Research* **51** (05): 2214-2226. http://dx.doi.org/10.1021/ie201872v.

Basheva, E. S., Ganchev, D., Denkov, N. D. et al. 2000. Role of Betaine as Foam Booster in the Presence of Silicone Oil Drops. *Langmuir* **16** (03): 1000-1013. http://dx.doi.org/10.1021/la990777.

Bian, Y., Penny, G. S. and Sheppard, N. C. 2012. Surfactant Formulation Evaluation for Carbon Dioxide Foam Flooding in Heterogeneous Sandstone Reservoir. Presented at the SPE Improved Oil Recovery Symposium, Tulsa, Oklahoma, 14-18 April. SPE 154018. http://dx.doi.org/10.2118/ 154018-MS.

Chen, Y., Elhag, A. S., Poon, B. M., et al 2012. Ethoxylated Cationic Surfactants for CO$_2$ EOR in High Temperature, High Salinity Reservoirs. Presented at the SPE Improved Oil Recovery Symposium, Tulsa, Oklahoma, 14-18 April. SPE 154222. http://dx.doi.org/10.2118/154222-MS.

Emrani, A. S., Ibrahim, A. F., and Nasr-El-Din, H. A. 2017. Mobility Control using Nanoparticle-Stabilized CO$_2$ Foam as a Hydraulic Fracturing Fluid. Presented at the SPE Europec featured at 79th EAGE Conference and Exhibition, Paris, France, 12-15 June. SPE-185863-MS. https://doi.org/10.2118/185863-MS.

Emrani, A. S., and Nasr-El-Din, H. A. 2017. An Experimental Study of Nanoparticle-Polymer-Stabilized CO$_2$ Foam. *Colloids and Surfaces, A: Physicochemical and Engineering Aspects*, **524** (01): 17-27.

Espinoza, D. A., Caldelas, F. M., Johnston, K. P., et al. 2010. Nanoparticle-Stabilized Supercritical CO$_2$ Foams for Potential Mobility Control Applications. Presented at the SPE Improved Oil Recovery Symposium, Tulsa, Oklahoma, 24-28 April. SPE 129925. http://dx.doi.org/10.2118/ 129925-MS.

Kalyanaraman, N., Arnold, C., Gupta, A., et al. 2016. Stability Improvement of CO$_2$ Foam for Enhanced Oil-Recovery Applications Using Polyelectrolytes and Polyelectrolyte Complex Nanoparticles. *Journal of Applied Polymer Science*, **134** (01):1-15. http://dx.doi.org/10.1002/app.44491.

Koczo, K., Lobo, L. A., and Wasan, D. T. 1992. Effect of Oil on Foam Stability: Aqueous Foams Stabilized by Emulsions. *Journal of Colloid and Interface Science* **150** (02): 492-506. DOI: http://dx.doi.org/10.1016/0021-9797(92)90218-B.

Mo, D., Yu, J., Liu, N., et al. 2012. Study of the Effect of Different Factors on Nanoparticle-Stablized CO_2 Foam for Mobility Control. Presented at the SPE Annual Technical Conference and Exhibition, San Antonio, Texas, 8-10 October. SPE 159282. http://dx.doi.org/10.2118/159282- MS.

Mohd, T. A. T., Shukor, M., Ghazali, N. et al. 2014. Relationship between Foamability and Nanoparticle Concentration of Carbon Dioxide (CO_2) Foam for Enhanced Oil Recovery (EOR). *Applied Mechanics and Materials*. **548** (01): 67-71. Trans Tech Publications.

San, J., Wang, S., Yu, J. et al., 2017. Nanoparticle-Stabilized Carbon Dioxide Foam Used in Enhanced Oil Recovery: Effect of Different Ions and Temperatures. *SPEJ*. Preprint. http://dx.doi.org/10.2118/179628-PA.

Singh, R., and Mohanty, K. K. 2014. Synergistic Stabilization of Foams by a Mixture of Nanoparticles and Surfactants. Presented at the Improved Oil Recovery Symposium, Tulsa, 12–16 April. SPE-169126-MS. https://doi.org/10.2118/169126-MS.

Xiao, C., Balasubramanian, S. N., and Clapp, L. W. 2016. Rheology of Supercritical CO_2 Foam Stabilized by Nanoparticles. Presented at the SPE Improved Oil Recovery Conference, Tulsa, Oklahoma, USA, 11-13 April. SPE-179621-MS. http://dx.doi.org/10.2118/179621-MS.

Xing, D., Wei, B., McLendon, W. J. et al. 2012. CO_2-Soluble, Nonionic, Water-Soluble Surfactants That Stabilize CO_2-in-Brine Foams. *SPE J.* **17** (04). http://dx.doi.org/10.2118/129907-PA.

Wang, C., and Li, H. Z. 2014. Foam Stability of Solvent/Surfactant/Heavy-Oil System under Reservior Conditions. Presented at the SPE International Heavy Oil Conference and Exhibition, 8-10 December, Mangaf, Kuwait. SPE-172888-MS. http://dx.doi:10.2118/172888-MS.

Wang, D., Hou, Q., Luo, Y., et al. 2015. Stability comparison between particles-stabilized foams and polymer-stabilized foams. *Journal of Dispersion Science and Technolog*y, **36** (2): 268-273.

Yin, G., Grigg, R. B., and Svec, Y. 2009. Oil Recovery and Surfactant Adsorption during CO_2-Foam Flooding. Presented at the Offshore Technology Conference, Houston, Texas, USA, 4-7 May. OTC-19787-MS. http://dx.doi:10.4043/19787-MS.

Yu, J., Liu, N., Li, L., et al. 2012. Generation of Nanoparticle-Stabilized Supercritical CO_2 Foams. Presented at the Carbon Management Technology Conference, Orlando, Florida, 7-9 February. CMTC 150849. http://dx.doi.org/10.7122/150849-MS.

Zhao, G., Fang, J., Dai, C. et al. 2015. Enhanced Foam Stability by Adding Dispersed Particle Gel: A New 3-Phase Foam Study. Presented at the SPE Asia Pacific Enhanced Oil Recovery Conference, Kuala Lumpur, Malaysia, 11-13 August. SPE-174597-MS. http://dx.doi:10.2118/174597-MS.